International Journal of Applied Earth Observation and Geoinformation 132 (2024) 104058

Contents lists available at ScienceDirect

International Journal of Applied Earth Observation and Geoinformation

journal homepage: www.elsevier.com/locate/jag

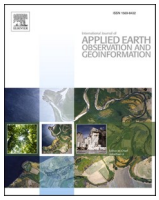

Measuring solar radiation and spatio-temporal distribution in different street network direction through solar trajectories and street view images

Lei Wang [a], Ce Hou [c], Yecheng Zhang [d], Jie He [a,b,*]

[a] School of Architecture, Tianjin University, Tianjin 300072, China
[b] School of Architecture, Harbin Institute of Technology, Shenzhen, Shenzhen 518055, China
[c] Department of Civil and Environmental Engineering, The Hong Kong University of Science and Technology, Clear Water Bay, Kowloon, 999075, Hong Kong, China
[d] School of Architecture, Tsinghua University, Beijing 100084, China

ARTICLE INFO

Keywords:
Solar radiation intensity
Street view images
Street directions
Deep learning
Street canyons

ABSTRACT

Under the dual pressures of rapid urbanization and global warming, the management of solar radiation has become an urgent issue to address. In this context, the potential regulatory role of urban street networks on solar radiation has garnered widespread attention. However, existing research lacks an understanding of the impact of street direction. By utilising street view data and solar trajectory simulation technology, it becomes possible to facilitate the revelation of spatiotemporal differences in solar radiation across streets with different direction. The results show that solar radiation is generally lower on north–south streets than on east–west streets. In terms of spatial differences, the average solar radiation in the fifth ring of Beijing is 25.38% higher than that in the second ring. Temporally, the average solar radiation in August, the highest month, is 15.98% greater than in October, the lowest month. Additionally, solar radiation on east–west street direction shows more intense variations in summer. A periodic variation in solar radiation was also discovered in relation to street angles, with different frequencies and amplitudes at 30° and 180°. This study is the first to focus on the directional attributes of roads at an urban scale. By utilising 100,000 street view images, it calculates and analyses the spatiotemporal distribution of solar radiation in Beijing during summer across different direction. The findings provide new insights into the relationship between the distribution of solar radiation and the morphology of urban roads.

1. Introduction

Every tree and building in a street shapes a unique microclimate environment under the influence of solar energy, constantly impacting the living experience of urban residents and their perception (Li, 2021). The amount of thermal radiation in street canyons will affect residents' preference for outdoor activities (Huang et al., 2015; Hwang et al., 2011; Jin et al., 2017; Lin et al., 2013). It is also a key parameter that influences human thermal comfort (Hodder and Parsons, 2006; Kurazumi et al., 2013). During the hot summer season, exposing to sunlight for a long time leads to the thermal discomfort for citizens and reduce their opportunity for outdoor activities (Hwang et al., 2011; Lin et al., 2013, 2010), which is a more urgent issue in the context of global warming. The extreme heatwave in summer will also have a significantly negative impacts on human well-being and daily life (Jin et al., 2017; Kurazumi et al., 2013). Therefore, understanding the spatio-temporal variations in solar radiation in high-density urban areas are crucial for creating livable and sustainable urban environments.

The study of the impact of urban built environment on urban solar radiation has attracted considerable interest in the fields of urban science and environmental science. Various studies have been conducted to explore and examine the relationship between various built environment factors and solar radiation in street canyons. For example, solar radiation in street canyons is influenced by factors such as sun trajectory, tree coverage, and the direction of street networks (Carrasco-Hernandez et al., 2015; Hwang et al., 2011; Johansson, 2006; Lin et al., 2013). Plants can absorb sunlight and undergo photosynthesis, as well as influence microclimates through evaporation of water (Onishi et al., 2010). Tall tree canopies can provide shade and prevent direct solar radiation on the ground (Armson et al., 2013). The geometric characteristics of urban roads, such as road density and intersection quantity, can influence human travel levels and preferences (Chen et al., 2022; Li et al., 2023). Areas with higher road accessibility typically have more shading facilities. Additionally, the radiation reaching the ground is also

* Corresponding author at: School of Architecture, Harbin Institute of Technology, Shenzhen, Shenzhen 518055, China
E-mail address: hejie2021@hit.edu.cn (J. He).

https://doi.org/10.1016/j.jag.2024.104058
Received 11 May 2024; Received in revised form 6 June 2024; Accepted 23 July 2024

influenced by building blocks within street canyons (Ali-Toudert and Mayer, 2006; Sanusi et al., 2016; Zhang et al., 2017). These studies highlight the importance of built environment elements such as vegetation, buildings, and roads, providing necessary insights for urban decision-makers.

In addition to analyzing the relevant factors that affect solar radiation, identifying and measuring of solar radiation efficient are also crucial. However, empirical research methods for measuring solar radiation rely on specialized equipment (Acuña Paz et al., 2021). Although empirical studies are highly reliable, they are time-consuming and cannot be conducted on a large scale. In addition, it is inaccurate to use solar radiation measurement in a small area to predict the whole urban area, especially some urban street canyons with very complex structure. Therefore, there is an urgent need for effective, accuracy, and reliable methods to measure and understand the spatio-temporal distribution solar radiation in urban environments.

In recent years, street view images have been proven to be a reliable tool for observing the urban built environment, providing a low-cost solution for on-site visual measurements, which is also shows a great potential for large-scale measurement and computation of solar radiation. Researchers have utilized street view images to study various urban phenomena and applications. For example, urban spatial perception measurement (Wang et al., 2022; Zhang et al., 2018), assessment of greening structures in street canyons (Sun et al., 2021; Zhang et al., 2023; Zhu et al., 2023), prediction of urban crime rates (Yao et al., 2023; Zhang, 2021), estimation of object positions in street canyons (Liu et al., 2023; Lumnitz et al., 2021), and analysis of the built environment (Gao et al., 2023; Liu and Liu, 2022). Meanwhile, the rapid development of computer science has facilitated the extraction of hidden features from street view images. For example, deep learning methods based on Transform have been developed to detect limb obstacles in urban areas (Hu et al., 2023). Building age prediction from street view images using publicly available government data has been achieved (Sun et al., 2022). Image semantic segmentation has been used to identify the colors of buildings in street views and generate color maps (Zhai et al., 2023).

In contrast to the gaps present in previous research, our work primarily addresses the following four research questions to enhance the understanding in the field of solar radiation and urban morphology:

1. How can the distribution of solar radiation be calculated using street view images that contain temporal and directional information?
2. What are the trends in solar radiation changes across different months of summer for streets direction in various directions?
3. Is there consistency in the changes of solar radiation across different street direction between inner and outer urban areas?
4. What insights do the distribution characteristics of solar radiation in different street direction offer for urban planning and environmental optimization?

The innovation of this study is mainly reflected in the following aspects: Firstly, it employs large-scale street view image data to provide a low-cost and highly efficient method for measuring solar radiation in different street orientations. Secondly, this work not only focuses on the spatial distribution of solar radiation but also delves into the temporal variation of radiation across different months of summer. Lastly, by introducing the analysis of periodic variations in street orientations, it reveals how minor changes in street angles significantly impact solar radiation, offering a new perspective for the refined management of urban thermal environments.

Specifically, we first collect panoramic street view images of nearly 100,000 street points in Beijing from May to October during the summer seasons from 2015 to 2022. These images represent the urban built environment. Next, we convert the panoramas into fisheye images and calculate the sun's trajectory within the fisheye images. By utilizing the National Solar Radiation Database, we accurately calculate the solar radiation for the entire city. Considering the spatiotemporal heterogeneity, it is crucial to differentiate the spatial and temporal distribution and mechanisms of solar radiation. To achieve this, we divide the space based on the boundaries of the city's fifth ring road and divide the time based on the summer months, allowing for an in-depth analysis of the variations in solar radiation and street network directions. These findings not only enrich the theoretical framework of solar radiation research but also provide practical guidance for urban planning and sustainable development.

2. Related works

2.1. Solar radiation simulation and calculation

With technological advancements, researchers have proposed and developed various methods and tools to calculate solar radiation levels within street canyon networks. Numerical simulation models can capture spatial heterogeneity variations (Gál and Kántor, 2020). Computational fluid dynamics (CFD) software models such as FLUENT have been widely used to study urban climate and solar radiation levels (Blocken, 2015). However, simulating cities in built environments (including buildings, vegetation, and public infrastructure) requires higher computational power and longer analysis time. Due to the high requirements for computer performance and computational costs, CFD models are difficult for non-experts to use or apply in large-scale urban models (Mirzaei, 2021). Another classic approach is based on remote sensing imagery to calculate parameters such as tree canopy coverage and vegetation indices to explain the microclimate regulation in urban street canyons (Chen et al., 2006; Kong et al., 2014b, 2014a). However, this method only reflects remote sensing imagery during a specific time period and cannot simulate the precise solar radiation values considering the complex canopy structure and accurate sun trajectory within street canyons. With the widespread availability of high-resolution digital model data, it has become possible to simulate precise solar radiation values within street canyons. However, these digital city models often do not include the canopy layer of street trees (Li et al., 2018).

Matzarakis et al., (2010) employed ground-based hemispherical images combined with field measurements to accurately measure solar radiation and thermal environment within urban street canyons. They demonstrated that ground-based hemispherical images serve as a valuable supplementary data source for simulating and measuring solar radiation within urban street canyons. The use of ground-based hemispherical images allows for better consideration of solar incidence angles. Building upon this, Li and Ratti measured solar radiation using urban street view images (Li and Ratti, 2019). In another study, the solar photovoltaic potential of urban roads was measured using street view images (Liu, 2019).

2.2. Influence of street network on thermal radiation

Urban morphological patterns, including street patterns and street density, influence urban functioning and microclimate (Li et al., 2023). However, due to various of natural environment, socio-economic environment, and historical planning, street network patterns. Existing research has shown that variations in street network patterns have significant influence for traffic safety (Marshall and Garrick, 2011), public health (Marshall et al., 2014), energy consumption (Mohajeri et al., 2015), and crime safety (Summers and Johnson, 2017). Previous studies have proposed various methods to identify street network patterns. Marshall (2004) defined five street types, which is linear, dendritic, radial, cell, and hybrid. Other studies have measured ring (Heinzle et al., 2006), grid (Yang et al., 2010), and complex changing patterns (Zhou and Li, 2015). More recently, entropy concepts have been employed to measure the global patterns (order or disorder) of street networks. Directional entropy, which measures the variation in street directions, is considered an important indicator of street network patterns and their associated urban forms. Directional entropy has been used to study 100

cities worldwide, revealing that cities in the United States and Canada resemble grid patterns more than other locations (Boeing, 2019). Coutrot et al. (2022) further explained human spatial direction abilities based on directional entropy.

Street networks have obvious influence on solar radiation. Theoretically, east–west- direction streets receive longer sunlight durations as they align with the direction of the sun's movement (Zhang et al., 2017). Studies have found that street trees distributed along east–west- direction streets provide stronger cooling effects for street canyon microclimates (Sanusi et al., 2016). Another study developed a three-dimensional urban surface model (3D-USM) for spatiotemporal simulation of climatic environments. It quantified the solar radiation levels varying with street directions, providing insights for effective urban cooling strategies in the face of urbanization and climate change (Yun et al., 2023). Existing research evidence indicates that long-term access to comfortable street spaces contributes to residents' physical activity (Hickman, 2013). Comfortable streets also enhance people's aesthetic appreciation of urban streets and can reduce personal stress (Carmona et al., 2018). The positive factors brought by high-quality streets have led scholars and urban planners in various fields to pay more attention to creating streets with a good sensory experience (Hagen and Tennøy, 2021). Therefore, considering the intensity of street radiation is a prerequisite for street renovation and reconstruction projects. Identifying the influence of street network directions on solar radiation helps understand the current state of urban development and study how different street network directions impact our urban climate and environment (Araújo De Oliveira, 2022).

3. Study area and data description

This study selects the urban area of Beijing City as the research area, primarily encompassing the area within the Fifth Ring Road (Fig. 1). The Fifth Ring Road serves as a boundary between the urban and suburban areas and is an important criterion for land use zoning. The research area enjoys abundant sunshine, with an annual average of 2000–2800 h of sunshine. Most of roads in the research area are in a north–south or east–west direction, exhibiting a relatively regular pattern (Yang et al., 2021). Additionally, the research area includes diverse types of urban canyons, including tall buildings and narrow alleyways, which contribute to the complexity of solar radiation conditions (Liu, 2019). All these factors make the analysis of solar radiation in Beijing an important issue.

We utilized Baidu Street View Images (BSVIs) as our source of street view data. Baidu, being one of the primary providers of street view data in China, offers comprehensive street view imagery covering almost the entire city of Beijing. They regularly update their data, making it one of the primary sources for street view research in the region (Biljecki and Ito, 2021).

Considering that plant growth is influenced by seasonal changes. The shedding of leaves in winter significantly impacts the results obtained through the solar trajectory method used in this study to measure solar radiation. Moreover, this research does not focus on comparing solar radiation levels between summer and winter. Therefore, we filtered and retained only the street view data for the summer period (May to October). We obtained the road network within the Fifth Ring Road of Beijing from OpenStreetMap (OSM) and used this road network data to create street view sampling points at 50-meter intervals (Fig. 1(c)), from which we obtained street view images. Following this method, we collected a total of 436,592 street view images from 157,732 sampling points, with each image captured as a panoramic view.

Next, we filtered the sampling points based on their acquisition time between May and October from 2015 to 2022 (Fig. 2(b)), resulting in a final dataset of 98,910 panoramic street view images that met our criteria. One of the main focal points of this study is the impact of street direction on solar radiation. By parsing the metadata, we can obtain the angle (Angle) between the direction of the car's movement and the geographic north direction in the spatial domain, as illustrated in Fig. 2.

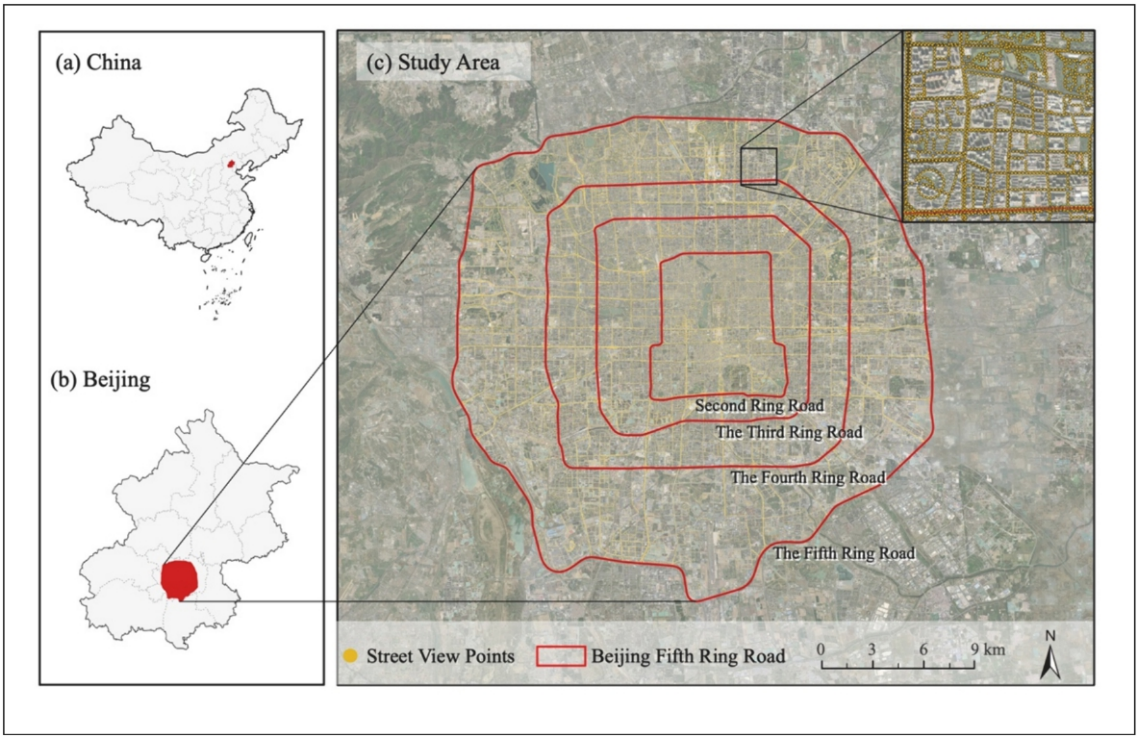

Fig. 1. Study area. (a)China, (b)Beijing, (c)Study area of Beijing fifth ring road.

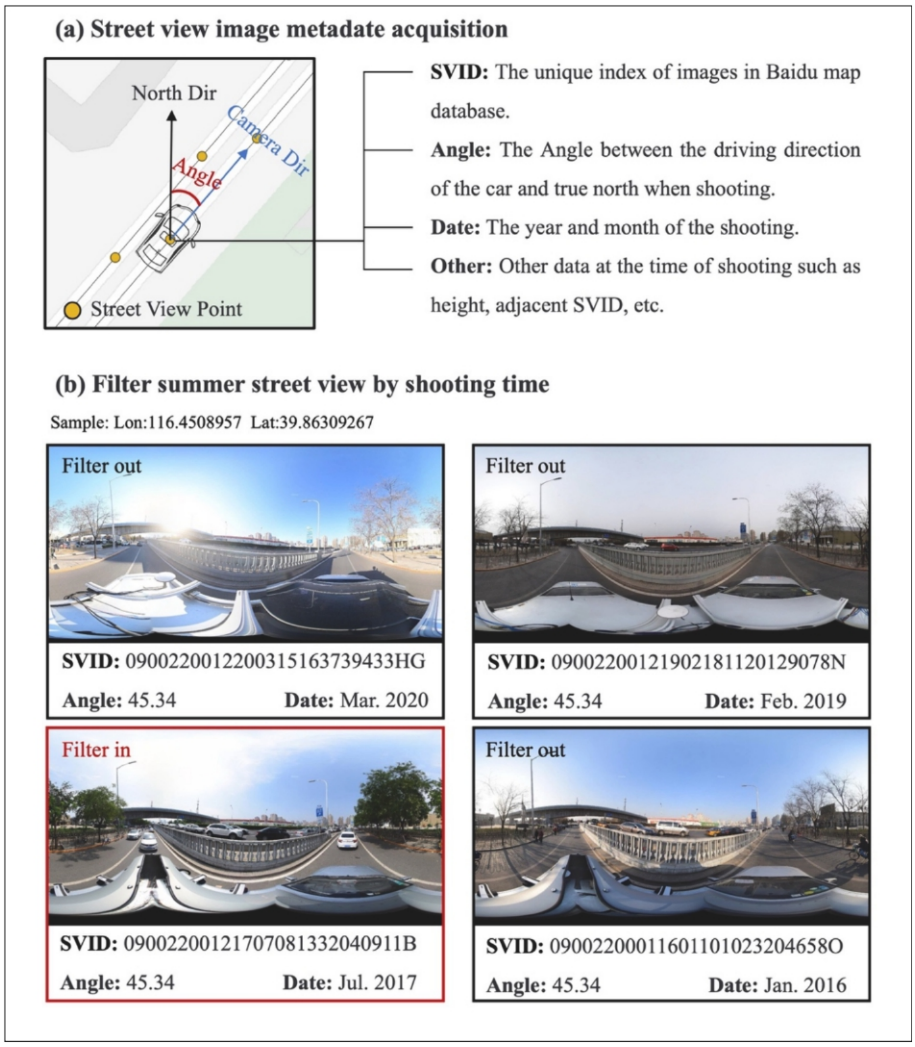

Fig. 2. Street view image metadata acquisition and filtering based on summer time. (a)Street view image metadate acquisition, (b)Filter summer street view by shooting time.

4. Methodology

4.1. Generation of fisheye image

The collection of panoramic street view images was accomplished by filtering based on season and year, while recording the metadata of each street view. To compute the sun trajectory, we converted these panoramic street view images from equidistant cylindrical projection to equidistant azimuthal projection, creating a fisheye image (Li and Ratti, 2019). This image conversion method is particularly suitable for this research as it can simplify complex urban environments into computable geometric models, thereby more accurately simulating the distribution of solar radiation on city streets. This conversion not only enhances the precision of calculating the solar trajectory but also enables us to more reliably predict the impact of different street direction on solar radiation reception. Specifically, by converting images into fisheye projections, we can more accurately analyze the interference of plant shadows and reflections on solar radiation, thus providing more reliable data support for the analysis.

The mathematical model for this transformation is detailed in Fig. 3 (a). Here, W_c and H_c represent the width and height of the panoramic image, so the radius of the fisheye image is given by $r0 = \frac{W_c}{2\pi}$, and the width and height of the fisheye image are $\frac{W_c}{\pi}$. Consequently, the center of the fisheye image (C_x, C_y) can be calculated using Eq. (1). For any pixel position (x_f, y_f) in the fisheye image, its corresponding pixel position (x_c, y_c) in the panoramic image can be obtained using Eq. (2).

$$C_x = C_y = \frac{W_c}{2\pi}\# \tag{1}$$

$$x_c = \frac{\theta}{2\pi}W_c y_c = \frac{r}{r_0}H_c\# \tag{2}$$

For any given coordinate (x_f, y_f) in the fisheye image, the angle θ with respect to the starting position and the radius r from the center can be calculated using Eqs. (3) and (4) respectively:

$$\theta = \begin{cases} \frac{3\pi}{2} - arctan\left(\frac{y_f - C_y}{x_f - C_x}\right), x_f < C_x \\ \frac{\pi}{2} - arctan\left(\frac{y_f - C_y}{x_f - C_x}\right), x_f > C_x \end{cases}\# \tag{3}$$

$$r = \sqrt{(x_f - C_x)^2 + \left(y_f - C_y\right)^2}\# \tag{4}$$

Based on the aforementioned model, the panoramic street view images are transformed into fisheye images. However, the resulting fisheye images do not have the actual north direction aligned at the top. Therefore, it is necessary to calculate the rotation angle based on the

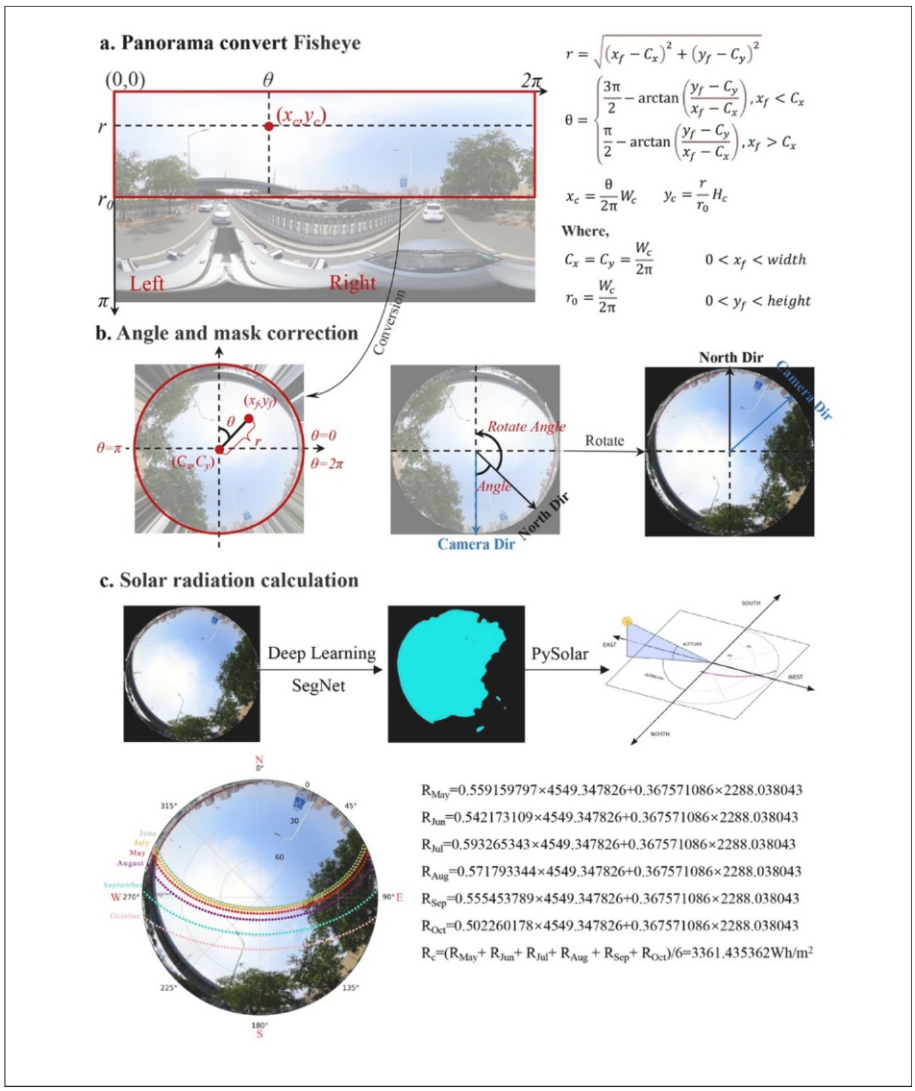

Fig. 3. Fisheye diagrams are used to calculate Solar Radiation and thermal comfort. (a)Panorama covert fisheye image formula, (b) example of fisheye image angle and mask correction, (c) the trajectory of the sun from May to October to calculate solar radiation.

camera's angle with respect to the north direction, as captured in the metadata. The rotation angle can be calculated using Eq. (5). The images are then processed using OpenCV tools to perform a counter-clockwise rotation, aligning the fisheye image's top towards the actual north direction in the geographical space (Fig. 2(c)).

$$RotateAngle = \begin{cases} 180 - Angle, Angle \leq 180 \\ 540 - Angle, Angle > 180 \end{cases} \# \quad (5)$$

In Eq. (5), *Angle* represents the angle derived from the metadata of the Baidu Street View panoramic image. The *Rotate Angle*, on the other hand, is the calculated angle for counter-clockwise rotation of the image using OpenCV (as shown in Fig. 2(c)). It is worth noting that since all images need to follow the same clockwise rotation direction, when Angle $>$ 180, we use 540 degrees instead of 360 degrees. This ensures that the rotated fisheye image and the sun trajectory have the same coordinate system in the 2D plane. This alignment enables the overlay of the sun trajectory on the fisheye image, facilitating the calculation of solar radiation in this study.

4.2. Calculation of solar radiation

The movement trajectory of the sun in the sky on a specific date can be calculated based on precise longitude and latitude coordinates. By overlaying the sun trajectory on the fisheye image, we can compute the direct and scattered solar radiation. This information is used to represent the solar radiation at that particular location. When calculating solar radiation, it is necessary to consider the sky's contribution to the fisheye image. Previous studies have employed threshold segmentation methods to identify the difference in pixel colors between vegetation and the sky. In our research, we utilize a sophisticated pretrained deep learning model (Zhou et al., 2018) (Fig. 3(c)) for image semantic segmentation. This model achieves an accuracy of 80.91 % in segmenting images, meeting the precision requirements for our study. Thus, we overlap the sun's movement trajectory with the fisheye image to measure the sun's exposure time. Fig. 3(c) illustrates the sun's movement trajectory for a single location in the year 2020, covering the period from May to October, with the middle 15 days of each month selected. The sun's position is calculated at 10-minute intervals along the trajectory. Our study assumes ideal conditions of clear weather and no cloud cover, which may cause some deviations from the actual physical environment of the city.

Solar radiation consists of two components: direct radiation and diffuse radiation (Anderson, 1964; Fu and Rich, 2002). Fisheye images generated from panoramic street view images can be used to reasonably predict solar radiation in urban streets (Rich, 1989). Therefore, in this

study, we utilize fisheye image data from recent years' summer seasons to calculate street radiation.

For direct radiation, we calculate it based on the intersection ratio between the sun's trajectory and the sky pixels in the fisheye image. The calculation process can be expressed by Eq. (6). In the equation, h_1 represents the sunrise time, h_2 represents the sunset time. θ_h denotes the solar zenith angle at time h. $B_h$represents whether the sun is obstructed at time h, which is represented as a boolean value of 0 or 1.

$$PD = \frac{\sum_{h=h_1}^{h_2} B_h \cdot \cos\theta_h}{\sum_{h=h_1}^{h_2} \cos\theta_h} \# \tag{6}$$

Diffuse radiation is the form of solar radiation that is scattered in the atmosphere. It can be estimated by considering the distribution of shading obstacles and the diffuse sky (Rich, 1989). Assuming a uniform distribution of diffuse radiation in the sky, the sky can be divided into an 8x16 grid to create a sky chart. The proportion of diffuse radiation reaching the ground can be predicted using Eq. (7). In the equation, $G_{a,z}$ represents the proportion of visible sky obtained from image semantic segmentation, $\theta_{a,z,2}$ and $\theta_{a,z,1}$ are the upper and lower boundaries of the sky sector, and θ_z is the solar zenith angle at the centroid of the sky sector.

$$PF = \frac{\sum_{a=0}^{15}\sum_{z=0}^{7} G_{a,z} \cdot \left(\cos\theta_{a,z,2} - \cos\theta_{a,z,1}\right) \cdot \cos\theta_z}{16} \# \tag{7}$$

The total radiation on a street can be calculated by adding the total direct radiation from the sun and the total diffuse radiation from the sun (Richards and Edwards, 2017). In Eq. (8), the total direct radiation from the sun (Rad_{di}) and the total diffuse radiation from the sun (Rad_{dif}) are calculated using unobstructed ground station data for a 24-hour period. This data is obtained from the National Solar Radiation Database (https://www.nrel.gov/rredc/). By using this data, we can calculate the average daily direct radiation and diffuse radiation in Beijing from May 1st to October 31st, 2020, which are 4549.34 Wh/m^2 and 2288.03 Wh/m^2, respectively.

$$R_{month} = PD \cdot Rad_{di} + PF \cdot Rad_{dif} \# \tag{8}$$

Finally, we calculate the average total solar radiation between May and October, represented by R_{may} and R_{oct} respectively. The average radiation over the five months is denoted as R_c in Eq. (9), which serves as an indicator for solar radiation.

$$R_c = \frac{R_{May} + R_{Jun.} + R_{Jul.} + R_{Aug.} + R_{Sep.} + R_{Oct.}}{6} \# \tag{9}$$

4.3. Street direction threshold

The specific quantification of street direction is depicted in Fig. 4. As mentioned earlier, we utilize metadata captured along with street views to determine the direction of the street network. When vehicles travel on north–south streets, the recorded angle data falls within three ranges: 0°<Angle < 30°, 150°<Angle < 210°, and 330°<Angle < 360°. To avoid ambiguity and facilitate calculations, we treat 360° and 0° as separate values. On the other hand, when vehicles travel on east–west streets, the recorded angle data falls within two ranges: 60°<Angle < 120° and 240°<Angle < 300°.

Our study area comprises a total of 98,910 street view points. To explore the inner and outer city divisions shown in Fig. 5, we divide the area based on the five concentric ring roads of Beijing. We then conduct street direction statistics for each region. For the street view points within the 5th Ring Road and 4th Ring Road, there are 44,686 points, with 17,555 points oriented in the north–south direction and 19,429 points oriented in the east–west direction, accounting for 82.76 % of valid data. Within the 4th Ring Road and 3rd Ring Road, there are 23,485 street view points, with 9,713 points oriented in the north–south direction and 10,805 points oriented in the east–west direction, accounting for 87.37 % of valid data. Within the 3rd Ring Road and 2nd Ring Road, there are 15,767 street view points, with 7,034 points oriented in the north–south direction and 7,263 points oriented in the east–west direction, accounting for 90.68 % of valid data. Within the 2nd Ring Road, there are 14,971 street view points, with 6,206 points oriented in the north–south direction and 8,122 points oriented in the east–west direction, accounting for 95.71 % of valid data.

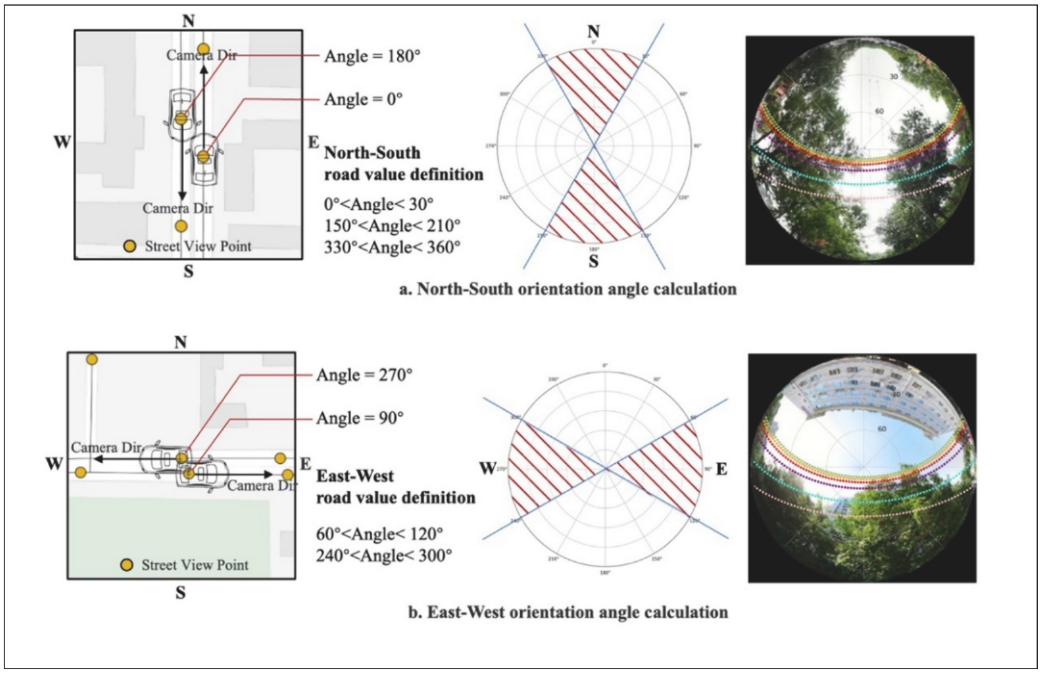

Fig. 4. Quantification and definition of road and fisheye street view direction. (a)North-South direction angle calculation, (b)East-West direction angle calculation.

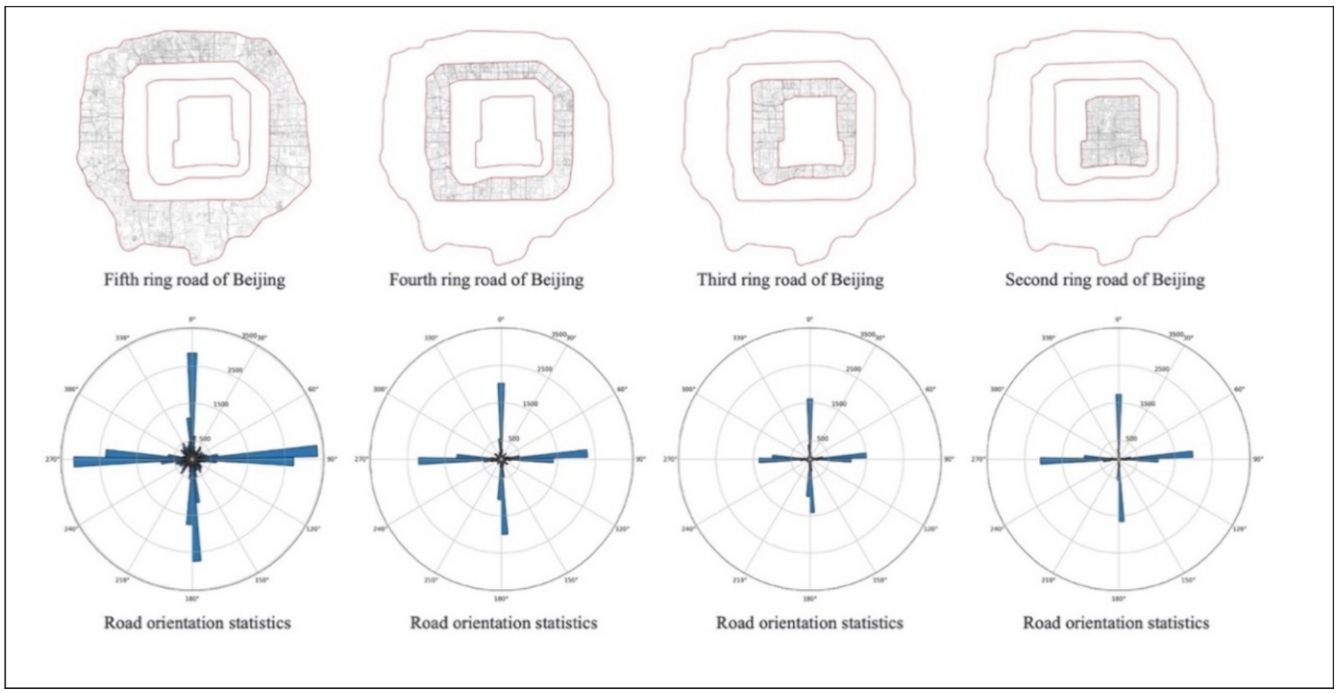

Fig. 5. Beijing five ring roads towards statistics.

5. Results

5.1. Spatial distribution of solar radiation under different street directions

The method we proposed enables the precise measurement of solar duration and solar radiation distribution at a city scale. In this study, in addition to quantitative analysis, we also investigated the spatial distribution of solar radiation in the urban areas. To visually display the geographical distribution of solar radiation, in Fig. 6 we show the geographical spatial level of solar radiation for each street view point. First, we remove the outliers where the solar radiation is zero from the data. Using the maximum and minimum values as the range, we apply the natural breaks classification method. We use a five-color gradient to represent different levels of solar radiation, with the gradient ranging from cool to warm tones. Cool tones represent the lowest level of solar radiation, while warm tones represent the highest level.

Fig. 6 on the left shows the spatial distribution of solar radiation at all street sampling points in the central urban area of Beijing. To visualize the spatial pattern more clearly, in Fig. 6 on the right, we further aggregated the site-level solar radiation into hexagonal grids with a diameter of 300 m by calculating their average values. Hexagonal grids with an average value of 0 were excluded. Hexagonal grids, compared to square grids, have more edges and can better represent the spatial aggregation of solar radiation.

Overall, the distribution of solar radiation in Beijing shows a pattern of higher radiation in the outer periphery, gradually decreasing towards

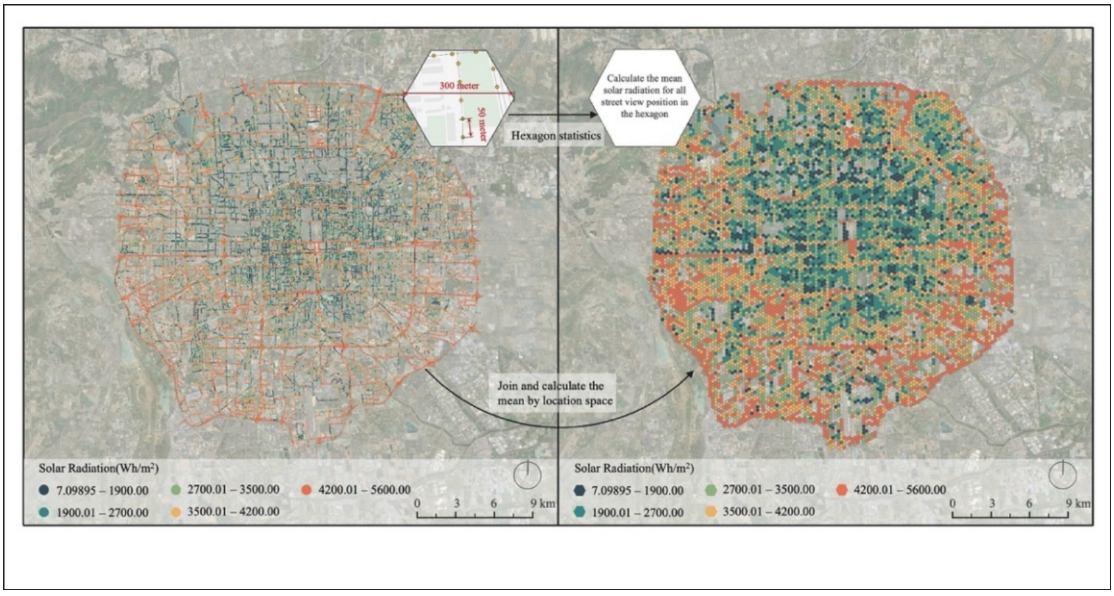

Fig. 6. Spatial distribution of solar radiation in Beijing Fifth Ring Road. In the left we used the original street view point coordinates. In the right, we use hexagons for mean statistics.

the inner side, and then increasing again towards the center. Additionally, the distribution of solar radiation exhibits clustering. The five concentric ring roads that divide Beijing show a relatively equal distribution of high solar radiation. There is a noticeable clustering of low solar radiation in the northern and northwestern parts of the city. The low solar radiation area in the north corresponds to the Beijing Olympic Forest Park, while the northwestern area is home to nearly 20 higher education institutions such as Tsinghua University and Beijing Forestry University. From the perspective of public service facilities, parks and the architectural blocks and green spaces of universities have a significant positive impact on reducing solar radiation. The central area of the city is occupied by Chang'an Avenue, with the street width reaching 48 m. The street width is a major factor leading to the higher solar radiation in the central area.

In order to discuss the impact of street network direction on the geographical distribution of solar radiation, we separately selected street sampling points in the north–south and east–west directions. In Fig. 7, the sampling points and hexagonal grid solar radiation for the two different directions are visualized. To achieve visual comparability, we also standardized the data classification rules. In Fig. 7(a), the overall solar radiation level of the north–south streets is significantly lower compared to the east–west streets in Fig. 7(b). From the comparison in the figure, it can be observed that the reduction of solar radiation in the inner city is more obvious in the north–south direction compared to the outer city. These spatial distributions are related to the development period of Beijing and indicate that the early-built communities in the inner city provide more street shading from buildings and vegetation, which have had a longer time to grow. In contrast, the reduction of solar radiation in the outer city, especially in the southwest direction of the southern region of Beijing, is more gradual. This indicates that the proportion of vegetation and buildings in the outer city changes less in the fisheye view, demonstrating that the trends in solar radiation variation reflect changes in the physical environment of certain areas. Analyzing the spatial distribution of solar radiation in these north–south and east–west streets helps consider the influence of the urban physical environment, thus providing insights into the complex mechanisms

Fig. 7. Geospatial distribution of Solar Radiation in different street network direction. (a)The distribution of Solar Radiation in the North-South street network, (b) The distribution of Solar Radiation in the West-East street network.

underlying these attributes.

Moreover, these differences significantly impact urban planning, development, and human behavior. For instance, the height and density of buildings can affect sunlight obstruction, leading to variations in solar radiation from different directions. Planners can utilize solar radiation data to optimize building layouts and the design of urban green spaces, as well as establish regulations on building heights to enhance energy efficiency and residential comfort. Furthermore, changes in sunlight duration and intensity may influence travel habits and outdoor activity schedules. Therefore, an in-depth exploration of the causes of solar radiation differences and their potential impacts on urban planning and human behavior will provide crucial scientific evidence for sustainable urban development.

5.2. Spatio-temporal variation of solar radiation

There is a significant spatial difference in solar radiation in different street directions during the summer in Beijing. In Fig. 8(b), we plotted the comparison of this difference. From the Fifth Ring Road to the Second Ring Road, the east–west streets have higher solar radiation than the north–south streets at different locations. Both directions also show an increasing trend of solar radiation from the inner city to the outer city. The average solar radiation in the Fifth Ring Road of Beijing is 25.38 % higher than that in the Second Ring Road. In Fig. 8(a), it can also be observed that in addition to the increasing trend of solar radiation, the standard deviation of radiation in the inner city is larger, while the radiation distribution in the outer city is more concentrated.

In Table 1, we compiled the data characteristics of solar radiation in different directions at various locations. For the Second Ring Road, the average solar radiation of north–south streets is 2634.92 Wh/m2, with a median of 2646.37 Wh/m2. In contrast, the average and median solar radiation of east–west streets are significantly higher, at 3301.79 Wh/m2 and 3574.13 Wh/m2, respectively. For the Third Ring Road, the average solar radiation of north–south streets is 2747.76 Wh/m2, while it is 3260.52 Wh/m2 for east–west streets. Both directions show an increase in solar radiation from the Second Ring Road to the Third Ring Road, but the east–west direction still remains significantly higher than the north–south direction. Moving to the Fourth Ring Road, the average solar radiation for north–south streets further increases to 3094.79 Wh/m2. In comparison, the average solar radiation for east–west streets is 3604.54 Wh/m2, indicating a larger disparity with the north–south direction. On the Fifth Ring Road, the average solar radiation reaches 3460.54 Wh/m2 for north–south streets, while it is 3982.89 Wh/m2 for east–west streets. This area represents the highest solar radiation among the four ring roads, particularly in the east–west direction.

Table 1
Spatial Variation in Solar Radiation (wh/m2) for Different Street Directions in Summer.

Spatial Location	Direction	Mean	Median	Min	Max	S.D.
Second ring road	N-S	2634.92	2646.37	0.0	5505.66	1194.95
	W-E	3301.79	3574.13	0.0	5494.95	1323.41
Third ring road	N-S	2747.76	2808.57	0.0	5570.65	1249.27
	W-E	3260.52	3544.90	0.0	5478.76	1320.32
Fourth ring road	N-S	3094.79	3146.82	0.0	5552.73	1153.47
	W-E	3604.54	3874.81	0.0	5521.99	1218.29
Fifth ring road	N-S	3460.54	3558.95	0.0	5624.31	1166.94
	W-E	3982.89	4221.56	0.0	5644.16	1107.99

By conducting a comparative analysis, we can clearly observe that solar radiation on north–south streets is generally lower than that on east–west streets, which is consistent with our previous research findings. Several factors contribute to the significant differences in solar radiation among different street directions:

1. **Urban history and development:** Beijing, as an ancient capital of China, has a long history of urban development, and the street layout is influenced by ancient planning. Early-built communities in the inner city typically have narrow streets and high building density, providing more shading and reducing solar radiation. In contrast, the streets and building layouts in the outer city are relatively newer, potentially resulting in higher solar radiation.
2. **Distribution and height of buildings:** Buildings in the city center are usually more dense and taller, which provides more shading for the streets and reduces solar radiation. In the outskirts, especially along the Fifth Ring Road, the distribution and height of buildings may differ from the inner city due to more relaxed land use regulations, leading to increased solar radiation.
3. **Vegetation coverage:** Vegetation can effectively absorb and diffuse solar radiation. The inner city has significant vegetation coverage, such as the Beijing Olympic Forest Park, which acts as a green shade umbrella for the city. Additionally, areas with abundant green spaces in university campuses contribute to a reduction in solar radiation.
4. **Street direction and physical environment:** Beijing's streets predominantly run in the north–south and east–west directions. Due to

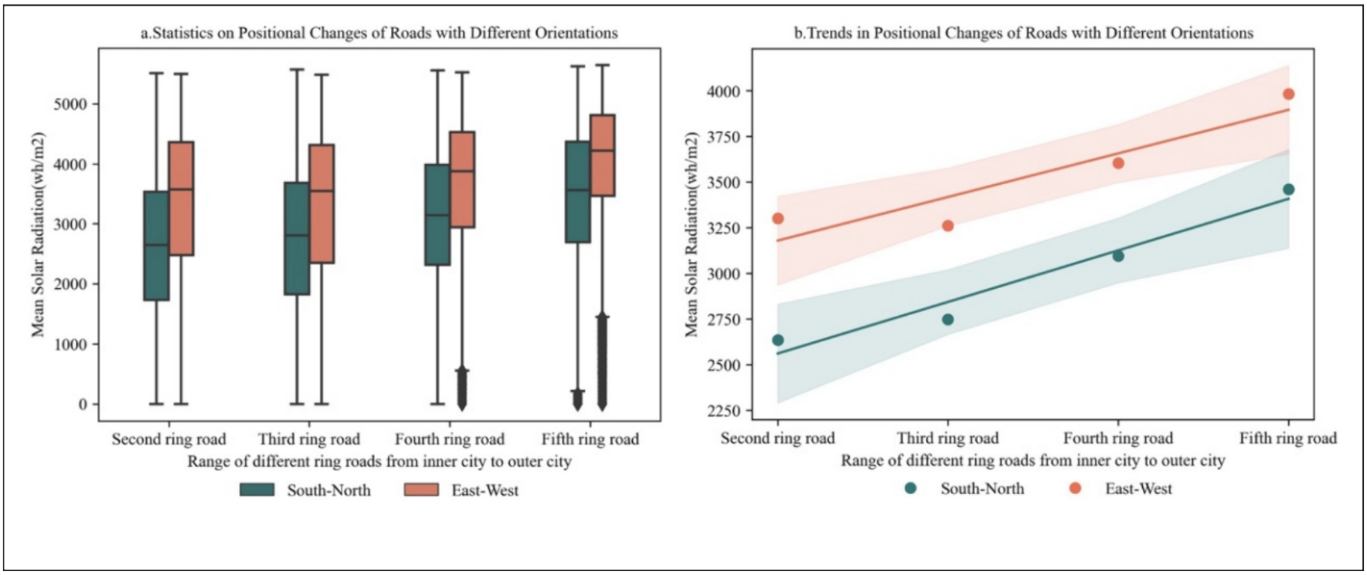

Fig. 8. Analysis of spatial variation of Solar Radiation with different street direction in summer.

the Earth's rotation and geographical location, north–south streets may often be in the shadow of buildings, resulting in reduced solar radiation for most of the day. East-west streets, on the other hand, are exposed to direct sunlight during morning and evening hours, leading to increased solar radiation.

5. **Specific regional characteristics:** For instance, Chang'an Avenue has a width of 48 m. Such wide streets allow more direct sunlight to reach the ground, leading to increased solar radiation.

These factors collectively contribute to the distinct variations in solar radiation among different street directions, providing insights into the complex mechanisms of urban physical environments.

5.3. Impact of street direction on solar radiation

In Beijing, there are also significant temporal differences in solar radiation for different street directions during the summer. In Fig. 9(b), we applied a quadratic curve fitting to illustrate this trend. Generally, east–west streets have higher solar radiation from May to September, but in October, there is a sudden decrease due to the change in the sun's trajectory. Overall, the solar radiation variation is more pronounced for east–west streets during the summer. On the other hand, the solar radiation changes more gradually for north–south streets. Additionally, as shown in Fig. 8(a), it can be observed that the standard deviation of solar radiation variation is greater for east–west streets, which results in a more variable perception of heat for urban residents on these streets.

In Table 2, we have compiled the data characteristics of solar radiation in different directions at various time periods. By examining the data for different months, we can observe the trends in solar radiation from May to October. For north–south streets, the average solar radiation is highest in August, while it is lowest in October. The solar radiation in August is 15.98 % higher compared to May. In contrast, for east–west streets, there is a noticeable decrease in solar radiation in October. This trend indicates that as the summer progresses, the solar radiation on the streets gradually decreases, following a pattern of initial increase and subsequent decrease. Furthermore, there are variations in the standard deviation of solar radiation among different street directions, suggesting differences in the variability of solar radiation. East-west streets exhibit higher variability in solar radiation during September and October.

When considering the periodic variation in street angles, our analysis must ensure the continuity of the fitted curve at both ends. To ensure a continuous fitting between 0° and 360°, we adopted a specific strategy

Table 2
Temporal Variation in Solar Radiation (wh/m2) for Different Street Directions in Summer.

Spatial Location	Direction	Mean	Median	Min	Max	S.D.
May	N-S	3143.71	3212.09	0.00	5691.53	1263.16
	W-E	3847.75	4188.11	0.00	5694.51	1228.61
June	N-S	3095.86	3158.62	0.00	5688.12	1257.42
	W-E	3719.77	4005.21	0.00	5694.04	1203.47
July	N-S	3108.52	3172.51	0.00	5684.82	1256.89
	W-E	3758.32	4060.04	0.00	5694.04	1208.67
Aug	N-S	3153.70	3236.93	0.00	5688.92	1258.70
	W-E	3894.39	4315.60	0.00	5693.93	1271.93
Sep	N-S	3152.47	3235.07	0.00	5691.65	1276.05
	W-E	3724.98	4231.68	0.00	5688.99	1510.26
Oct	N-S	3081.21	3149.57	0.00	5696.96	1277.71
	W-E	2996.83	3167.51	0.00	5691.30	1647.49

to expand the data set from −30° (330°) to 390° (30°). Subsequently, the plotted curve range was truncated to 0° to 360°. The formula is as follows:

$$Angle_{new} = \begin{cases} Angle - 360^{\circ}, 330^{\circ} \le Angle \le 180^{\circ} \\ Angle + 360^{\circ}, 0^{\circ} \le Angle \le 30^{\circ} \end{cases} \# \quad (10)$$

In Eq. (10), "Angle" represents the angles in the original data set, and "Anglenew" represents the expanded data set. We take the data between 330° and 360° and subtract 360° from the corresponding angles to obtain new data ranging from −30° to 0°. Similarly, we take the data between 0° and 30°, and add 360° to the corresponding angles to obtain new data ranging from 360° to 390°. However, when plotting Fig. 10, we only display the range from 0° to 360°.

As shown in Fig. 10(a), we analyze the quantified data of street directions and solar radiation in a two-dimensional coordinate system for each streetscape point. Each grey dot represents a street view point , the x-axis represents the street direction angles corresponding to the streetscape points, while the y-axis represents the computed solar radiation values. Similar to the distribution of the street network in Beijing, the streetscape points are predominantly distributed in the north–south and east–west directions. The solar radiation levels are significantly lower in the north–south directions (0°/360° and 180°) on the y-axis compared to the east–west directions (90° and 270°). It's worth noting that besides the primary distribution in the four main directions, there are also minor distribution angles indicated by red boxes

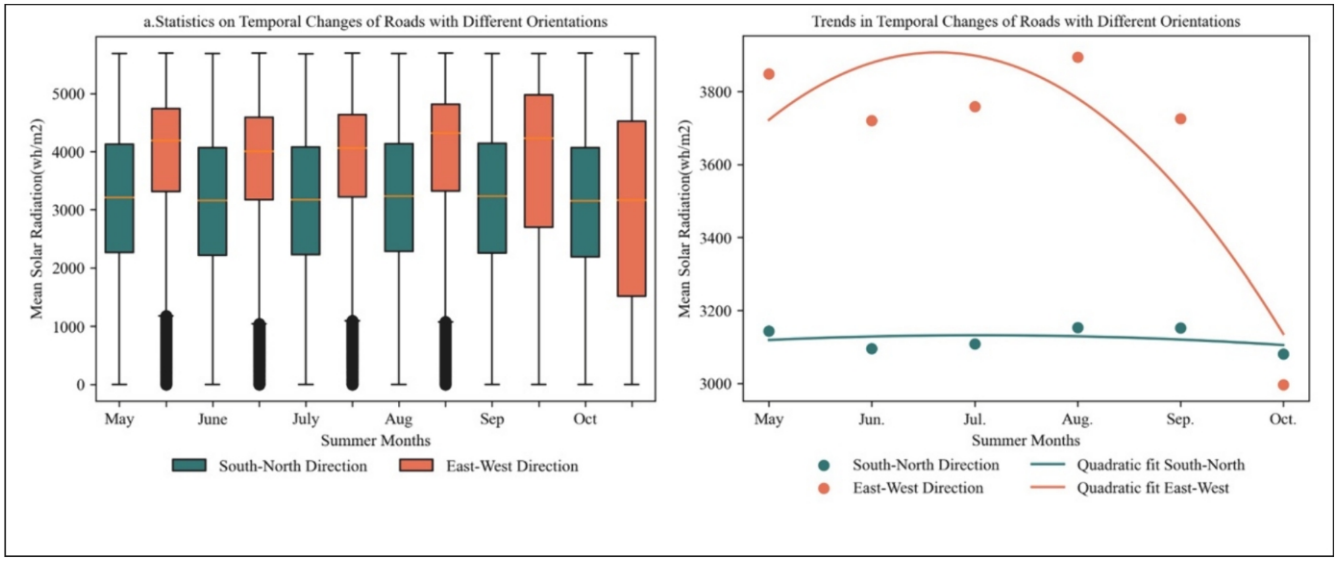

Fig. 9. Analysis of time variation of Solar Radiation with different street direction in summer.

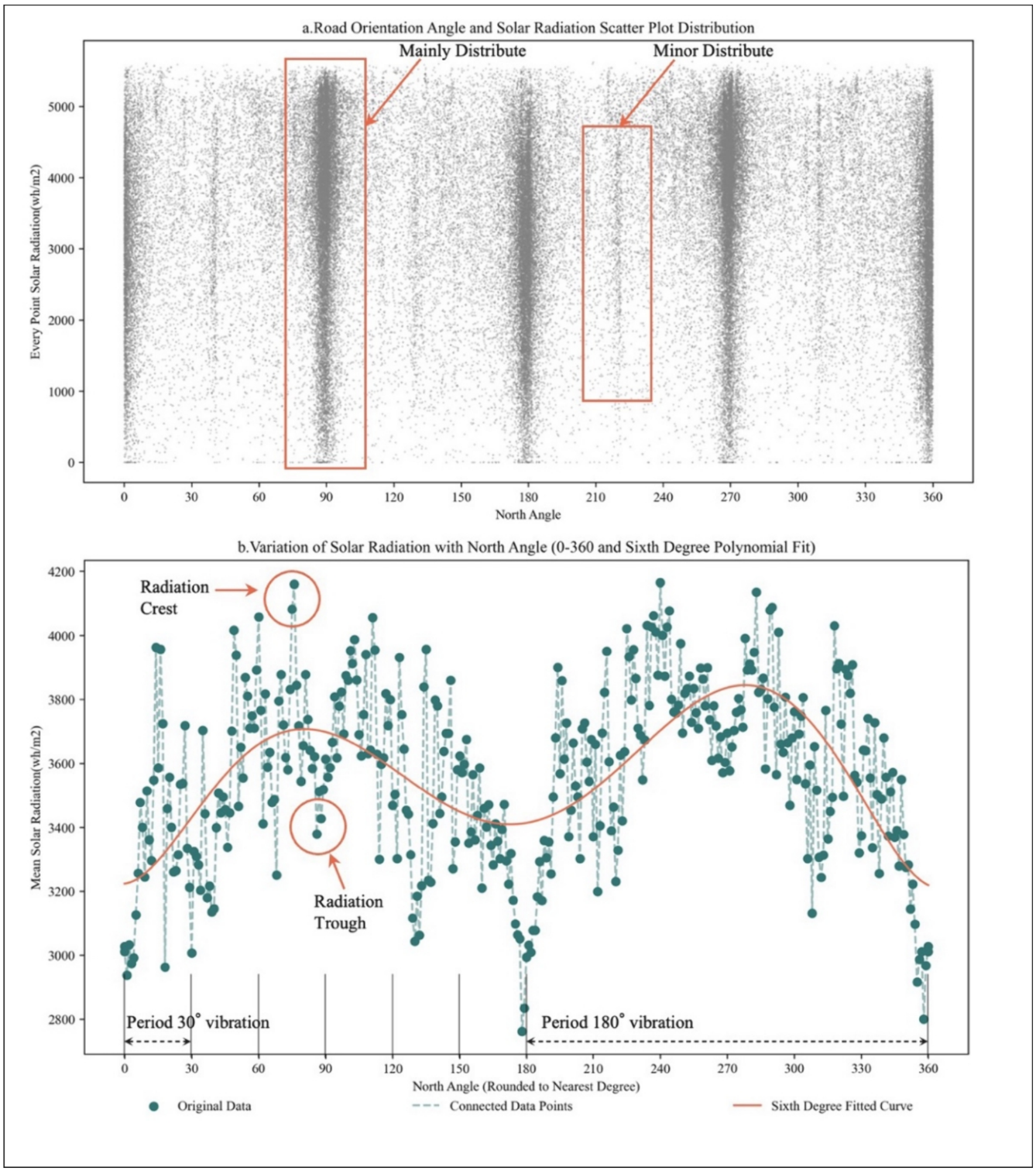

Fig. 10. Correlation analysis of street network direction Angle and Solar Radiation. (a)The Angle and Solar Radiation of each street view are plotted to visually show the distribution, (b) Analyze of the periodic change of Solar Radiation with increasing Angle.

in the figure. These angles occur at approximately 30°, 130°, 220°, and 310°, which align with the street layout in Beijing. Streets in these four angle directions serve as connections between the east–west and north–south directions.

Fig. 10(b) analyzes the six-degree polynomial fitting curves for the average relative solar radiation variation within each one-degree angle. We compiled and calculated the mean solar radiation represented by all the grey dots within a one-degree angle, with this mean value indicated by solid green dots. Similarly, the x-axis represents the corresponding street direction angles of the mean values, and the y-axis represents the calculated mean solar radiation. We then connect them with dashed lines of the same color, depicting the overall variation of solar radiation across all street direction angles in the city. To smooth out the process, we employ a six-degree polynomial curve for fitting. The fitting results show that the troughs of the polynomial curve are in the north–south directions, with two troughs occurring in these directions. Interestingly,

we can observe more variation cycles besides the two peaks and troughs, which are worth noting and can be further analyzed using Fourier transform. In the entire vibration frequency, there are two major vibration frequency curves. Each of these curves contains multiple vibrations within the two cycles, occurring at 0° (180°), 30° (210°), 60° (240°), 90° (270°), 120° (300°), 150° (330°), and 180° (360°).

From this, we can observe an interesting phenomenon. Starting from 0°, every 30° increase represents one vibration cycle. Although the vibration curve at 30° in the figure is not perfectly regular, we can still identify a certain pattern. As the street direction angle changes, every six small vibration cycles form a complete solar radiation variation cycle. Therefore, the increase in solar radiation from north-south roads to east–west roads is not linear but rather periodic and gradually increasing. These findings provide a novel perspective for understanding the relationship between street directions and solar radiation.

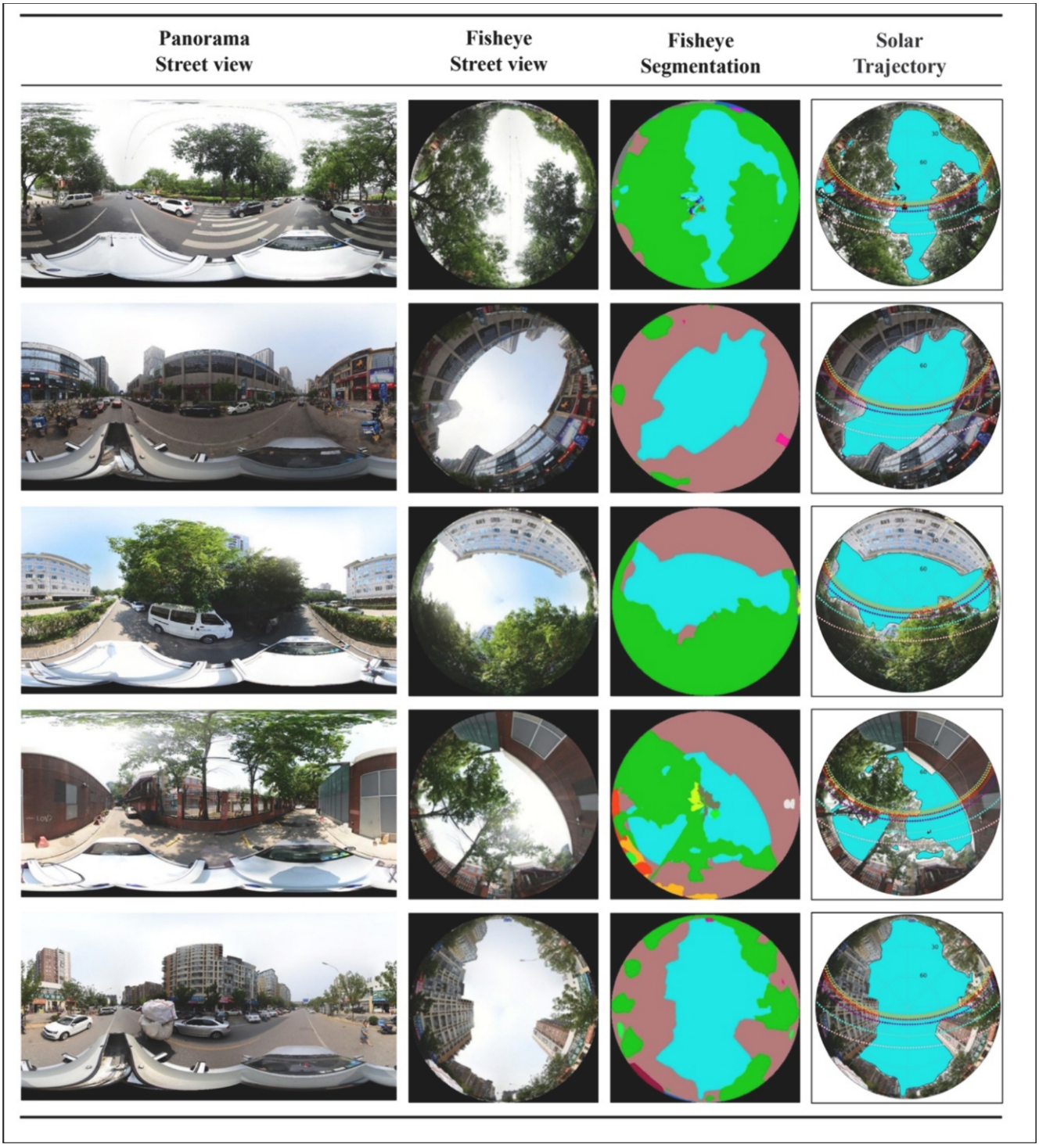

Fig. 11. Selected samples of calculating solar radiation from a street view panorama with different street network direction.

6. Discussion

6.1. Summary of the research phenomenon

As shown in Fig. 11, we calculated the solar radiation in different directions of urban street spaces using panoramic street view data and traced the path of the sun. Based on the computational results, this study revealed the geographic spatial distribution and temporal variation of solar radiation at the city scale, particularly in metropolitan areas like Beijing. Through in-depth analysis of the relationship between street network directions and solar radiation, several key phenomena were observed. Firstly, the solar radiation distribution in Beijing exhibited significant heterogeneity in geographic space, with pronounced differences in solar radiation intensity between the central area and the periphery. This distribution pattern was closely related to factors such as the city's building layout, green coverage, and street width. For example, Beijing's central axis, Chang'an Avenue, due to its unique width and historical significance, had noticeably higher solar radiation intensity compared to other areas. Secondly, the directional nature of streets had a significant impact on solar radiation. In Beijing, north–south streets generally received lower solar radiation compared to east–west streets, which was attributed to the Earth's axis of rotation and Beijing's specific geographic location, resulting in more time spent in the shadow of buildings for north–south streets. Additionally, from a temporal perspective, the intensity of solar radiation was influenced not only by seasonal factors but also by street direction. In summer, the variation in solar radiation intensity was more pronounced between different months for east–west streets, while it remained relatively stable for north–south streets. This phenomenon revealed the need for urban planning to consider seasonal and temporal changes when optimizing residents' perception of radiation by street layout. Finally, through the analysis of the correlation between street angles and solar radiation, it was found that there was periodic variation in solar radiation with street angles. This phenomenon indicated that even small changes in street direction could have a significant impact on solar radiation, thereby affecting the daily lives of city residents.

Different directions of solar radiation also have various other impacts on the urban environment. For example, in the rental and real estate markets, properties facing north or south usually command higher prices. This is because residents believe that such directions provide longer exposure to sunlight, enhancing the living experience in the rooms. However, from a building design perspective, walls facing the west receive intense sunlight in the summer, leading to higher indoor temperatures. These findings provide valuable insights for urban planning and management, emphasizing the importance of considering solar radiation in street design and reconstruction. Particularly in the context of global warming and the exacerbation of urban heat island effects, they offer more targeted strategies for sustainable development in cities worldwide.

6.2. Policy implications for urban development

With the acceleration of urbanization, considering residents' thermal perception and quantifying management of solar radiation in urban design and planning has become an urgent task. This study provides us with an in-depth understanding of the variations of solar radiation in different street directions and over time, thereby offering valuable insights for urban policymakers and planners.

Importance of urban history and development: The intertwining of Beijing's ancient city structure with the processes of modernization, particularly the differences in solar radiation between the inner and outer city, provides an interesting revelation. It highlights the pivotal role of urban history and development trajectories in influencing the distribution of solar radiation. Therefore, when considering future urban planning, it is essential to value the preservation of the city's historical and cultural heritage while ensuring that new development projects harmonize with the existing urban structure and environment.

Integration of green spaces and architectural design: This study emphasizes the impact of vegetation and buildings on solar radiation. To optimize the radiation status of cities, we should encourage the integration of green spaces and architectural design in urban planning. For example, measures such as increasing urban green areas, rooftop greening, and vertical greening can be implemented. Enhancing greening in fundamental public facilities like campuses and parks can effectively influence solar radiation and provide a more comfortable living environment for urban residents.

Comprehensive consideration of street direction and physical environment: Considering the significant influence of street direction on solar radiation, future urban planning should pay more attention to the relationship between street direction and the physical environment. For instance, north–south streets may be more suitable for high-density buildings to provide more shading and reduce solar radiation, while east–west streets may require more green spaces and open areas to influence solar radiation.

Human Activities and Housing Prices:Research indicates that the direction of a house directly impacts its energy consumption and living comfort. For instance, houses facing south can receive more solar heat during winter, thus reducing the demand for heating and improving energy efficiency. Consequently, such houses often command higher prices in the market. Conversely, houses facing north, while they avoid excessive direct sunlight in summer and reduce the frequency of air conditioning use, receive less natural light and are not favored by homebuyers. Additionally, street direction significantly affects human activity patterns. If urban public spaces can effectively utilize solar radiation direction, the outdoor activity experience of citizens can be significantly enhanced. For example, greenways and squares facing southeast can provide ample sunlight in the morning, which not only promotes morning exercise among citizens but also increases the frequency of use of these public spaces. These examples fully illustrate the importance of solar radiation and street orientation in the housing market and human activities. Future research could further quantify these impacts and explore how to better utilize the analysis results in urban planning and architectural design to improve residents' quality of life and urban sustainability.

7. Research limitations and future works

However, there are limitations to this study. It primarily focuses on the summer season and may not account for variations in solar radiation during other seasons. Besides street direction, urban development, and vegetation coverage, there are many other factors that can influence solar radiation, such as cloud cover and atmospheric pollution. While polynomial fitting and Fourier transform can describe certain characteristics of the data, they may oversimplify and fail to capture all the nuances.

In future research, it is equally important to supplement and refine the distribution of solar radiation for other seasons to obtain a comprehensive annual perspective for analysis. Expanding the study area to verify the research conclusions is also crucial. By measuring different urban morphologies, more precise patterns of how street direction affects solar radiation distribution can be discovered. With continuous technological advancements, especially the development of deep learning models, these advanced technologies can significantly improve the description and prediction of solar radiation distribution.

In this field of study, we can introduce deep learning models such as Convolutional Neural Networks (CNN) and Long Short-Term Memory networks (LSTM) to analyze and process complex solar radiation data. These models have significant advantages in capturing nonlinear relationships and spatiotemporal features within the data, thereby enhancing prediction accuracy. Furthermore, deep learning technology can integrate multi-source data, including meteorological data, satellite images, and historical radiation data, to provide more comprehensive

and detailed radiation distribution predictions. Future research could further explore how to optimize these models to achieve high-precision predictions of solar radiation distribution, thereby providing stronger support for related fields.

8. Conclusion

This study delves into the impact of street network direction on solar radiation in high-density metropolises like Beijing, China. We found that the distribution of solar radiation is significantly influenced by street direction in terms of geographic spatial distribution. Solar radiation is higher in areas closer to the urban periphery compared to the inner city. In terms of temporal distribution during the summer, there are significant variations in solar radiation intensity along east–west streets, while north–south streets exhibit relatively stable patterns. Through correlation analysis between street direction and solar radiation, we discovered periodic patterns, which provide valuable insights for urban planning and design. By analyzing large-scale street-level data, this study offers a more detailed and comprehensive geographic spatial distribution map of solar radiation. It reveals the close relationship between street direction, especially in the north–south and east–west directions, and solar radiation, which aids in the construction of people-centric cities. Additionally, this paper analyzes how factors such as Beijing's urban development history, building distribution and height, and vegetation coverage affect solar radiation. By employing polynomial fitting and Fourier transform, this study reveals the periodic patterns between solar radiation and street direction.

CRediT authorship contribution statement

Lei Wang: Writing – review & editing, Writing – original draft, Visualization, Methodology, Formal analysis, Data curation, Conceptualization. **Ce Hou:** Writing – review & editing, Writing – original draft, Software, Methodology. **Yecheng Zhang:** Writing – review & editing, Writing – original draft, Software, Methodology, Formal analysis, Conceptualization. **Jie He:** Validation, Supervision, Project administration, Funding acquisition.

Declaration of competing interest

The authors declare that they have no known competing financial interests or personal relationships that could have appeared to influence the work reported in this paper.

Data availability

The code and sample dataset used in this research have been released openly on https://github.com/LandscapeWL/SHAPClab_SolarRadiation_StreetOrientation.

Acknowledgements

Supported by the Research Initiative Fund for Newly Introduced Talents of Harbin Institute of Technology, Shenzhen. 2023-2025 (#ZX20230488)

References

Acuña Paz, Y., Miño, J., Duport, N., Beckers, B., 2021. Pixel-by-pixel rectification of urban perspective thermography. Remote Sensing of Environment 266, 112689. https://doi.org/10.1016/j.rse.2021.112689.

Ali-Toudert, F., Mayer, H., 2006. Numerical study on the effects of aspect ratio and orientation of an urban street canyon on outdoor thermal comfort in hot and dry climate. Building and Environment 41, 94–108. https://doi.org/10.1016/j.buildenv.2005.01.013.

Anderson, M.C., 1964. Studies of the Woodland Light Climate: I. The Photographic Computation of Light Conditions. Journal of Ecology 52, 27–41. https://doi.org/10.2307/2257780.

Araújo De Oliveira, V.M., 2022. Urban Morphology: An Introduction to the Study of the Physical Form of Cities, The Urban Book Series. Springer International Publishing, Cham. doi: 10.1007/978-3-030-92454-6.

Armson, D., Asrafur Rahman, M., Roland Ennos, A., 2013. A Comparison of the Shading Effectiveness of Five Different Street Tree Species in Manchester. UK. AUF 39. https://doi.org/10.48044/jauf.2013.021.

Biljecki, F., Ito, K., 2021. Street view imagery in urban analytics and GIS: A review. Landscape and Urban Planning 215, 104217. https://doi.org/10.1016/j.landurbplan.2021.104217.

Blocken, B., 2015. Computational Fluid Dynamics for urban physics: Importance, scales, possibilities, limitations and ten tips and tricks towards accurate and reliable simulations. Building and Environment 91, 219–245. https://doi.org/10.1016/j.buildenv.2015.02.015.

Boeing, G., 2019. Urban spatial order: street network orientation, configuration, and entropy. Appl Netw Sci 4, 67. https://doi.org/10.1007/s41109-019-0189-1.

Carmona, M., Gabrieli, T., Hickman, R., Laopoulou, T., Livingstone, N., 2018. Street appeal: The value of street improvements. Progress in Planning 126, 1–51. https://doi.org/10.1016/j.progress.2017.09.001.

Carrasco-Hernandez, R., Smedley, A.R., Webb, A.R., 2015. Using urban canyon geometries obtained from Google Street View for atmospheric studies: Potential applications in the calculation of street level total shortwave irradiances. Energy and Buildings 86, 340–348.

Chen, L., Lu, Y., Ye, Y., Xiao, Y., Yang, L., 2022. Examining the association between the built environment and pedestrian volume using street view images. Cities 127, 103734. https://doi.org/10.1016/j.cities.2022.103734.

Chen, X.-L., Zhao, H.-M., Li, P.-X., Yin, Z.-Y., 2006. Remote sensing image-based analysis of the relationship between urban heat island and land use/cover changes. Remote Sensing of Environment 104, 133–146. https://doi.org/10.1016/j.rse.2005.11.016.

Coutrot, A., Manley, E., Goodroe, S., Gahnstrom, C., Filomena, G., Yesiltepe, D., Dalton, R.C., Wiener, J.M., Hölscher, C., Hornberger, M., Spiers, H.J., 2022. Entropy of city street networks linked to future spatial navigation ability. Nature 604, 104–110. https://doi.org/10.1038/s41586-022-04486-7.

Fu, P., Rich, P.M., 2002. A geometric solar radiation model with applications in agriculture and forestry. Computers and Electronics in Agriculture 37, 25–35. https://doi.org/10.1016/S0168-1699(02)00115-1.

Gál, C.V., Kántor, N., 2020. Modeling mean radiant temperature in outdoor spaces, A comparative numerical simulation and validation study. Urban Climate 32, 100571. https://doi.org/10.1016/j.uclim.2019.100571.

Gao, J., Ma, S., Wang, L., Shuai, L., Du, H., 2023. Does greenness bring more green travelling? Evidence from free-floating bike-sharing in Beijing. Journal of Transport Geography 109, 103586. https://doi.org/10.1016/j.jtrangeo.2023.103586.

Hagen, O.H., Tennøy, A., 2021. Street-space reallocation in the Oslo city center: Adaptations, effects, and consequences. Transportation Research Part d: Transport and Environment 97, 102944. https://doi.org/10.1016/j.trd.2021.102944.

Heinzle, F., Anders, K.-H., Sester, M., 2006. Pattern Recognition in Road Networks on the Example of Circular Road Detection, in: Raubal, M., Miller, H.J., Frank, A.U., Goodchild, M.F. (Eds.), Geographic Information Science, Lecture Notes in Computer Science. Springer, Berlin, Heidelberg, pp. 153–167. doi: 10.1007/11863939_11.

Hickman, C., 2013. 'To brighten the aspect of our streets and increase the health and enjoyment of our city': The National Health Society and urban green space in late-nineteenth century London. Landscape and Urban Planning 118, 112–119. https://doi.org/10.1016/j.landurbplan.2012.09.007.

Hodder, S.G., Parsons, K., 2006. The effects of solar radiation on thermal comfort. Int J Biometeorol 51, 233–250. https://doi.org/10.1007/s00484-006-0050-y.

Hu, C., Jia, S., Zhang, F., Xiao, C., Ruan, M., Thrasher, J., Li, X., 2023. UPDExplainer: An interpretable transformer-based framework for urban physical disorder detection using street view imagery. ISPRS Journal of Photogrammetry and Remote Sensing 204, 209–222. https://doi.org/10.1016/j.isprsjprs.2023.08.017.

Huang, K.-T., Lin, T.-P., Lien, H.-C., 2015. Investigating Thermal Comfort and User Behaviors in Outdoor Spaces: A Seasonal and Spatial Perspective. Advances in Meteorology 2015, 1–11. https://doi.org/10.1155/2015/423508.

Hwang, R.-L., Lin, T.-P., Matzarakis, A., 2011. Seasonal effects of urban street shading on long-term outdoor thermal comfort. Building and Environment 46, 863–870. https://doi.org/10.1016/j.buildenv.2010.10.017.

Jin, Y., Kang, J., Jin, H., Zhao, J., 2017. Analysis of Thermal Environment of Open Community Streets in Winter in Northern China. Energy Procedia 134, 423–431. https://doi.org/10.1016/j.egypro.2017.09.595.

Johansson, E., 2006. Influence of urban geometry on outdoor thermal comfort in a hot dry climate: A study in Fez, Morocco. Building and Environment 41, 1326–1338. https://doi.org/10.1016/j.buildenv.2005.05.022.

Kong, F., Yin, H., James, P., Hutyra, L.R., He, H.S., 2014a. Effects of spatial pattern of greenspace on urban cooling in a large metropolitan area of eastern China. Landscape and Urban Planning 128, 35–47. https://doi.org/10.1016/j.landurbplan.2014.04.018.

Kong, F., Yin, H., Wang, C., Cavan, G., James, P., 2014b. A satellite image-based analysis of factors contributing to the green-space cool island intensity on a city scale. Urban Forestry & Urban Greening 13, 846–853. https://doi.org/10.1016/j.ufug.2014.09.009.

Kurazumi, Y., Kondo, E., Ishii, J., Sakoi, T., Fukagawa, K., Bolashikov, Z.D., Tsuchikawa, T., Matsubara, N., Horikoshi, T., 2013. Effect of the Environmental Stimuli upon the Human Body in Winter Outdoor Thermal Environment. Journal of Environmental and Public Health 2013, 1–10. https://doi.org/10.1155/2013/418742.

Li, X., 2021. Investigating the spatial distribution of resident's outdoor heat exposure across neighborhoods of Philadelphia, Pennsylvania using urban microclimate

modeling. Sustainable Cities and Society 72, 103066. https://doi.org/10.1016/j.scs.2021.103066.
Li, X., Ratti, C., 2019. Mapping the spatio-temporal distribution of solar radiation within street canyons of Boston using Google Street View panoramas and building height model. Landscape and Urban Planning 191, 103387. https://doi.org/10.1016/j.landurbplan.2018.07.011.
Li, X., Ratti, C., Seiferling, I., 2018. Quantifying the shade provision of street trees in urban landscape: A case study in Boston, USA, using Google Street View. Landscape and Urban Planning 169, 81–91. https://doi.org/10.1016/j.landurbplan.2017.08.011.
Li, Y., Zhang, Y., Wu, Q., Xue, R., Wang, X., Si, M., Zhang, Y., 2023. Greening the concrete jungle: Unveiling the co-mitigation of greenspace configuration on PM2.5 and land surface temperature with explanatory machine learning. Urban Forestry & Urban Greening 88, 128086. https://doi.org/10.1016/j.ufug.2023.128086.
Lin, T.-P., Matzarakis, A., Hwang, R.-L., 2010. Shading effect on long-term outdoor thermal comfort. Building and Environment 45, 213–221. https://doi.org/10.1016/j.buildenv.2009.06.002.
Lin, T.-P., Tsai, K.-T., Liao, C.-C., Huang, Y.-C., 2013. Effects of thermal comfort and adaptation on park attendance regarding different shading levels and activity types. Building and Environment 59, 599–611. https://doi.org/10.1016/j.buildenv.2012.10.005.
Liu, Z., 2019. Towards feasibility of photovoltaic road for urban traffic-solar energy estimation using street view image. Journal of Cleaner Production 16.
Liu, D., Jiang, Y., Wang, R., Lu, Y., 2023. Establishing a citywide street tree inventory with street view images and computer vision techniques. Computers, Environment and Urban Systems 100, 101924. https://doi.org/10.1016/j.compenvurbsys.2022.101924.
Liu, Y., Liu, Y., 2022. Detecting the city-scale spatial pattern of the urban informal sector by using the street view images: A street vendor massive investigation case. Cities 131, 103959. https://doi.org/10.1016/j.cities.2022.103959.
Lumnitz, S., Devisscher, T., Mayaud, J.R., Radic, V., Coops, N.C., Griess, V.C., 2021. Mapping trees along urban street networks with deep learning and street-level imagery. ISPRS Journal of Photogrammetry and Remote Sensing 175, 144–157. https://doi.org/10.1016/j.isprsjprs.2021.01.016.
Marshall, W.E., Garrick, N.W., 2011. Does street network design affect traffic safety? Accident Analysis & Prevention 43, 769–781. https://doi.org/10.1016/j.aap.2010.10.024.
Marshall, W.E., Piatkowski, D.P., Garrick, N.W., 2014. Community design, street networks, and public health. Journal of Transport & Health 1, 326–340. https://doi.org/10.1016/j.jth.2014.06.002.
Matzarakis, A., Rutz, F., Mayer, H., 2010. Modelling radiation fluxes in simple and complex environments: basics of the RayMan model. Int J Biometeorol 54, 131–139. https://doi.org/10.1007/s00484-009-0261-0.
Mirzaei, P.A., 2021. CFD modeling of micro and urban climates: Problems to be solved in the new decade. Sustainable Cities and Society 69, 102839. https://doi.org/10.1016/j.scs.2021.102839.
Mohajeri, N., Gudmundsson, A., French, J.R., 2015. CO2 emissions in relation to street-network configuration and city size. Transportation Research Part d: Transport and Environment 35, 116–129. https://doi.org/10.1016/j.trd.2014.11.025.
Onishi, A., Cao, X., Ito, T., Shi, F., Imura, H., 2010. Evaluating the potential for urban heat-island mitigation by greening parking lots. Urban Forestry & Urban Greening 9, 323–332. https://doi.org/10.1016/j.ufug.2010.06.002.
Rich, P.M., 1989. A manual for analysis of hemispherical canopy photography (No. LA-11733-M). Los Alamos National Lab. (LANL), Los Alamos, NM (United States). doi: 10.2172/7064866.
Richards, D.R., Edwards, P.J., 2017. Quantifying street tree regulating ecosystem services using Google Street View. Ecological Indicators 77, 31–40. https://doi.org/10.1016/j.ecolind.2017.01.028.
Sanusi, R., Johnstone, D., May, P., Livesley, S.J., 2016. Street Orientation and Side of the Street Greatly Influence the Microclimatic Benefits Street Trees Can Provide in Summer. J. Environ. Qual. 45, 167–174. https://doi.org/10.2134/jeq2015.01.0039.
Summers, L., Johnson, S.D., 2017. Does the Configuration of the Street Network Influence Where Outdoor Serious Violence Takes Place? Using Space Syntax to Test Crime Pattern Theory. J Quant Criminol 33, 397–420. https://doi.org/10.1007/s10940-016-9306-9.
Sun, Y., Wang, X., Zhu, J., Chen, L., Jia, Y., Lawrence, J.M., Jiang, L., Xie, X., Wu, J., 2021. Using machine learning to examine street green space types at a high spatial resolution: Application in Los Angeles County on socioeconomic disparities in exposure. Science of the Total Environment 787, 147653. https://doi.org/10.1016/j.scitotenv.2021.147653.
Sun, M., Zhang, F., Duarte, F., Ratti, C., 2022. Understanding architecture age and style through deep learning. Cities 128, 103787. https://doi.org/10.1016/j.cities.2022.103787.
Wang, L., Han, X., He, J., Jung, T., 2022. Measuring residents' perceptions of city streets to inform better street planning through deep learning and space syntax. ISPRS Journal of Photogrammetry and Remote Sensing 190, 215–230. https://doi.org/10.1016/j.isprsjprs.2022.06.011.
Yang, N., Jiang, L., Chao, Y., Li, Y., Liu, P., 2021. Influence of Relief Degree of Land Surface on Street Network Complexity in China. IJGI 10, 705. https://doi.org/10.3390/ijgi10100705.
Yang, B., Luan, X., Li, Q., 2010. An adaptive method for identifying the spatial patterns in road networks. Computers, Environment and Urban Systems 34, 40–48. https://doi.org/10.1016/j.compenvurbsys.2009.10.002.
Yao, Y., Dong, A., Liu, Z., Jiang, Y., Guo, Z., Cheng, J., Guan, Q., Luo, P., 2023. Extracting the pickpocketing information implied in the built environment by treating it as the anomalies. Cities 143, 104575. https://doi.org/10.1016/j.cities.2023.104575.
Yun, S.H., Lee, D.K., Piao, Z.G., Park, C.Y., Kim, S.H., Kim, E.S., 2023. Developing a three-dimensional urban surface model for spatiotemporal analysis of thermal comfort with respect to street direction. Sustainable Cities and Society 97, 104721. https://doi.org/10.1016/j.scs.2023.104721.
Zhai, Y., Gong, R., Huo, J., Fan, B., 2023. Building Façade Color Distribution, Color Harmony and Diversity in Relation to Street Functions: Using Street View Images and Deep Learning. IJGI 12, 224. https://doi.org/10.3390/ijgi12060224.
Zhang, F., 2021. "Perception bias": Deciphering a mismatch between urban crime and perception of safety. Landscape and Urban Planning 14.
Zhang, Y., Du, X., Shi, Y., 2017. Effects of street canyon design on pedestrian thermal comfort in the hot-humid area of China. Int J Biometeorol 61, 1421–1432. https://doi.org/10.1007/s00484-017-1320-6.
Zhang, L., Wang, L., Wu, J., Li, P., Dong, J., Wang, T., 2023. Decoding urban green spaces: Deep learning and google street view measure greening structures. Urban Forestry & Urban Greening 87, 128028. https://doi.org/10.1016/j.ufug.2023.128028.
Zhang, F., Zhou, B., Liu, L., Liu, Y., Fung, H.H., Lin, H., Ratti, C., 2018. Measuring human perceptions of a large-scale urban region using machine learning. Landscape and Urban Planning 180, 148–160. https://doi.org/10.1016/j.landurbplan.2018.08.020.
Zhou, B., Zhao, H., Puig, X., Xiao, T., Fidler, S., Barriuso, A., Torralba, A., 2018. Semantic Understanding of Scenes through the ADE20K Dataset.
Zhou, Q., Li, Z., 2015. Experimental analysis of various types of road intersections for interchange detection. Transactions in GIS 19, 19–41. https://doi.org/10.1111/tgis.12077.
Zhu, H., Nan, X., Yang, F., Bao, Z., 2023. Utilizing the green view index to improve the urban street greenery index system: A statistical study using road patterns and vegetation structures as entry points. Landscape and Urban Planning 237, 104780. https://doi.org/10.1016/j.landurbplan.2023.104780.